DOI: 10.1002/ ((please add manuscript number))
Article type: Full Paper

Template-free, Surfactant-Mediated Orientation of Self-Assembled Supercrystals of Metal-Organic Framework Particles

Civan Avci, Yang Liu, Jose Angel Pariente, Alvaro Blanco, Cefe Lopez, Inhar Imaz,* Daniel Maspoch**

Dr. C.A., Y.L., Dr. I.I., Prof. D.M., Catalan Institute of Nanoscience and Nanotechnology (ICN2), CSIC and the Barcelona Institute of Science and Technology. Campus UAB, Bellaterra, 08193 Barcelona, Spain

Prof. D. Maspoch, ICREA, Pg. Lluís Companys 23, Barcelona, 08010, Spain

J.A.P., Dr. A.B., Prof. C.L., Materials Science Factory, Instituto de Ciencia de Materiales de Madrid (ICMM), Consejo Superior de Investigaciones Científicas (CSIC), Calle Sor Juana Inés de la Cruz, 3, 28049 Madrid, Spain

[+] C.A. and Y.L contributed equally to this work.

Keywords: Metal-Organic Framework, mesoscale assembly, supercrystal, crystal orientation, photonic crystals

Mesoscale self-assembly of particles into supercrystals is important for the design of functional materials such as photonic and plasmonic crystals. However, while much progress has been made in self-assembling supercrystals adopting diverse lattices and using different types of particles, controlling their growth orientation on surfaces has received limited success. Most of the latter orientation control has been achieved via templating methods in which lithographic processes are used to form a patterned surface that acts as a template for particle assembly. Herein we describe a template-free method to self-assemble (111)-, (100)- and (110)-oriented face-centered cubic supercrystals of the Metal-Organic Framework (MOF) ZIF-8 particles by adjusting the amount of surfactant (CTAB) used. We show that these supercrystals behave as photonic crystals whose properties depend on their growth orientation. This control on the orientation of supercrystals made of porous particles might ultimately facilitate pore orientation on surfaces for designing membranes and sensors.

The physical and even chemical properties of crystals often differ with crystal orientation,[1] due to the distinct atomic interactions and bond distances along the crystal directions, which can strongly affect the electronic, mechanical and/or magnetic characteristics. Accordingly, the integration of crystals into devices requires control of their surface orientation. [2] For instance, the importance of controlled growth of oriented crystalline (111)-silicon and (0001)-ZnO nanowires,[3,6] (001)-YBCO superconductors[4] and phosphorene semiconductors[5] on surfaces in electronic, photovoltaic and photonic devices has been described. To date, crystal orientation is controlled chiefly via direct-growth methods, including vapor/liquid/solid,[7] oxide-assisted[8] and template-based growth methods.[9]

Controlled orientation of crystals on surfaces can also improve the performance of porous materials integrated into devices or membranes. For example, Tsapatsis *et al.* demonstrated that zeolite ZSM-5 membranes in the (010)-orientation perform better at separation of xylene isomers than those in other orientations do. They attributed this advantage to the larger, straighter pores accessible along the *b*-axis throughout the membrane thickness, compared to the narrower, sinusoidal pores along the *a*-axis.[10] Likewise, MFI-type zeolite membranes in the (010)-orientation showed better separation performance and mass transfer than those in other orientations did.[11] Similar trends are expected for Metal-Organic Frameworks (MOFs), an emerging class of porous materials that can be synthesized in various shapes and pore sizes and that show extremely large surface areas and tailored internal surfaces.[12,13] Preliminary advances in controlling the orientation of MOF crystal growth on surfaces have been reported by Biemi *et al.*,[14] for HKUST-1 and by Zacher *et al.*,[15] for MOF-5, using *in situ* growth crystallization methods on substrates functionalized with self-assembled monolayers; and by Shekhah and Eddaoudi,[16] for ZIF-8, using layer-by-layer liquid phase epitaxy growth on substrates functionalized with self-assembled monolayers. Moreover, Falcaro *et al*. recently demonstrated the heteroepitaxial growth of centimeter-scale-oriented MOF films using crystalline copper hydroxide-covered silicon as a template substrate.[17]

Remarkably, when a fluorescent dye was adsorbed in the MOF crystals, these pore-oriented MOF films exhibited optical response as "ON/OFF" switching upon film rotation.

The earliest methods to control the orientation of MOF crystals rely on their coherent growth to form a continuous film of a given orientation.[14-17] We recently reported that colloidal crystals of ZIF-8 can self-assemble into centimeter-scale supercrystals on surfaces to create a structured film of singular building blocks with internal and inter-particle available porosity.[18] Supercrystals are often referred as three-dimensional well-ordered assemblies formed by colloidal crystalline particles[19,20] that, in the case of ZIF-8, are truncated rhombic dodecahedral (TRD) crystals of controllable truncation. In these supercrystals, whose particles are single-crystalline and faceted, every constituent ZIF-8 crystal has the same orientation. This observation prompted us to hypothesize that supercrystal formation could serve as an alternative to the aforementioned direct-growth methods for controlling the orientation of porous crystals on surfaces.

Herein we develop this approach by controlling the growth orientation of a face-centered-cubic (fcc) supercrystal assembled from TRD ZIF-8 crystals (truncation t = 0.63). Previous studies on the formation of fcc supercrystals with an orientation different from the most common one ((111)–oriented) are limited. In these few studies, fcc supercrystals (typically, (100)-oriented) were assembled via templating methods in which lithographic processes are exploited to form a patterned substrate that acts as a template for particle assembly.[21-23] In our new method described here, we report that orientation of fcc supercrystals can be controlled with the surfactant cetyltrimethylammonium bromide (CTAB); same used for the synthesis of TRD ZIF-8 crystals. This template-free approach enabled us to generate (111)-, (100)- and (110)-oriented ZIF-8 supercrystals (**Figure 1**), in which all the constituent ZIF-8 crystals are oriented along the <111>, <100> and <110> crystallite directions, respectively. This property implies that in the (111)-oriented supercrystals, the ZIF-8 particles with the largest pore apertures are aligned perfectly perpendicular to the surface.

-Figure 1-

We first chose to study TRD ZIF-8 particles in which the truncation value (t) = $2x/(\phi + x) = 0.63$ (where ϕ is the distance between opposing square facets, and x is the side of the square facets), as these particles self-assemble into fcc supercrystals.[16] The particles were synthesized by adding a solution of $ZnAc_2 \cdot 2H_2O$ (300 mg) in 5 mL of water to a solution of 1.56 g of 2-methylimidazole (2-MiM) and 0.40 mg of CTAB in 5 mL of water. The resulting transparent mixture was gently stirred for 15 s, causing it to evolve into a white colloidal suspension, which was left undisturbed at room temperature for 2 h. The resulting ZIF-8 particles were washed three times with deionized water upon centrifugation at 9000 rpm in 50 mL Falcon tubes. Field-emission scanning electron microscopy (FESEM) images revealed the formation of TRD particles of the following dimensions for $t = 0.63$: size (ϕ) = 233 ± 14 nm, and edge-length of square facets (x) = 106 ± 8 nm (Figure S1, Supporting Information). The size polydispersity of ZIF-8 particles was *ca.* 6% (Figure S1, Supporting Information). A powder X-ray diffraction (PXRD) pattern of the as-synthesized particles confirmed the formation of pure ZIF-8 (Figure S2, Supporting Information). An N_2 sorption isotherm taken at 77 K confirmed the porosity and indicated a BET surface area of 1215 m^2/g (Figure S3, Supporting Information).

We next performed an initial self-assembly experiment, in which we re-dispersed the synthesized particles in water (50 mg/mL). A droplet of 40 µL of this dispersion was placed on a polydimethylsiloxane (PDMS) coated SEM pin, which was then heated in an oven at 120 ^oC for 3 min until the droplet fully evaporated. Note here that the substrate was covered with PDMS to provide better homogeneity and robustness to the supercrystals, facilitating their handling, as they become slightly attached to the PDMS surface. Upon evaporation, a round-shaped, colorful ZIF-8 monolith was obtained with a diameter of *ca.* 6 mm. The monoliths obtained this way exhibited structural green color visible to the naked eye, signaling the formation of an ordered assembly. FESEM images revealed the formation of the (entropically favored) (111)-

oriented fcc plastic supercrystal, in which all TRD ZIF-8 particles are oriented with their <111> direction perpendicular to the surface of the monolith and thus, parallel to its (111) direction (Figure 1a). PXRD analysis of a (111)-oriented fcc supercrystal assembled on a silicon sample holder of the PXRD instrument showed the typical ZIF-8 pattern, with its highest intensity peak at $2\theta = 16^{o}$ (**Figure 2**). This peak corresponds to diffraction from the (222) plane of ZIF-8 (*i.e.* parallel to the (111) planes of the supercrystal), and thus confirmed the orientation of the ZIF-8 particles along the <111> direction. Hence, in this (111)-oriented supercrystal, the larger pore apertures (3.4 Å) connecting the 11.6 Å-in-diameter cavities of ZIF-8 running along the <111> direction are vertically aligned.

-Figure 2-

We next studied the possible influence of the surfactant CTAB on the self-assembly of TRD ZIF-8 particles. Specifically, we sought conditions that would provide alternate growth directions. Thus, we systematically prepared a series of dispersions of ZIF-8 particles at a concentration of 50 mg/mL, in which we stepwise increased the concentration of CTAB from 1.00 mg/mL to 4.00 mg/mL, and then studied the resulting supercrystal growth. At 1.00 mg/mL, results similar to that of the supercrystals self-assembled without addition of CTAB were obtained: the entire sample was (111)-oriented (Figure S4, Supporting Information). When the CTAB concentration was increased to 2.00 mg/mL, the formation of (100)-oriented domains on the perimeter of the monolith, and (111)-oriented domains in the center, were observed (Figure S5, Supporting Information). Upon increasing the CTAB concentration further, these (100)-oriented domains grew and became more abundant, gradually propagating towards the center. By a CTAB concentration of 3.00 mg/mL, a homogeneous (100)-oriented fcc supercrystal had been assembled (Figure 1b). Remarkably, the PXRD pattern of the (100)-oriented supercrystals showed its highest intensity peak at $2\theta = 11^{o}$, corresponding to the

diffraction from (002) planes of ZIF-8 (Figure 2c). This observation confirmed that the ZIF-8 particles forming this supercrystal were oriented along the <100> direction. Again, the crystallite orientation was parallel to that of the supercrystal.

When increasing the CTAB concentration up to 3.25 mg/mL, we began observing the formation of (110)-oriented domains. As previously, these new (110)-oriented domains started occurring on the perimeter of the monolith (Figure S7, Supporting Information) and propagated towards the center for increasing CTAB concentration. Although a purely (110)-oriented supercrystal could not be obtained filling the entirety of the monolith, even at a CTAB concentration of 4.00 mg/mL, the FESEM images of supercrystals obtained at this CTAB concentration revealed formation of a large, homogeneous, (110)-oriented area (Figure 1c), together with some (100)-oriented domains near the center of the monolith (Figure S8, Supporting Information). For the (110)-oriented crystals, PXRD showed a strong (twofold) reinforcement of the preferential Bragg diffraction (Figure 2d), as in the (111) and (100) orientations.

Snapshots of the self-assembly process of ZIF-8 supercrystals revealed that the droplet surface had become opalescent after only 20 seconds of incubation (Figure S9, Supporting Information). This opalescence in turn suggested that the supercrystal formation begins at the droplet interface, meaning that the self-assembly of ZIF-8 particles evolves from the droplet surface through the inside of the droplet.[24] It also suggested that the first layer of ZIF-8 particles that assembles at this interface governs further three-dimensional self-assembly. In fact, this assisted colloidal self-assembly resembles the colloidal epitaxy method, in which patterned substrates usually act as templates to direct the three-dimensional colloidal crystallization.[25] One intriguing question that remains is how CTAB directs the formation of the first (111)-, (100)- or (110)-layer. Considering a spherical particle, the planar packing fraction of the hexagonal (111) plane is 0.907, whereas those packing fractions of the (100) and (110) planes are 0.785 and 0.555, respectively. Thus, an increase in CTAB favors formation of

less-dense layers. Certain factors must be considered in this CTAB-dependence. Firstly, introduction of more positive charges in the dispersion can cause an increase in the number of repulsive interactions during ZIF-8 particle assembly. Secondly, formation of CTAB micelles, and/or a decrease in the droplet surface tension, can each alter particle assembly.

To validate the role of the surfactant (i.e. charge in the dispersion, micelles and the droplet surface tension), we investigated the use of another surfactant such as the anionic sodium dodecyl suphate (SDS) to control the self-assembly of ZIF-8 particles (Figure S10, Supporting Information). We observed completely disordered assemblies at SDS concentrations lower than 2 mg/mL, whereas ordered (111)-oriented supercrystals were obtained upon increasing the SDS concentration from 2 to 5 mg/mL. When increasing the SDS concentration up to 6 mg/mL, we started detecting the formation of (110)-oriented domains. These results further evidenced the importance of the surfactant concentration to change the growth orientation of these fcc ZIF-8 supercrystals.

In addition to enabling control over pore-channel direction, the orientation of fcc supercrystals also determines the photonic properties.[26] Accordingly, we next sought to study how changes in CTAB concentration might influence the photonic behavior of our MOF supercrystals. These supercrystals are periodic dielectric structures comprising ZIF-8 particles (size: ~230 nm); thus, they exhibit angle-dependent iridescence that is visible to the naked eye and that originates from a photonic band structure. We observed that increasing the CTAB concentration from 1 mg/mL to 3 mg/mL led not only to a shift in supercrystal orientation, from (111)-oriented to (100)-oriented, but also to a concomitant change in color from green to blue (**Figure 3**a), thus providing preliminary evidence of a shift in photonic properties. To further corroborate that the photonic behavior was orientation-dependent, we characterized both pure (111)- and (100)-oriented supercrystals with UV-Visible reflectance spectrometry to determine their respective photonic band gaps. Interestingly, unlike the other orientations, the (110)-oriented supercrystal did not show any similar iridescence. This was probably due to poor

crystal quality and/or to the heterogeneity of the entire monolith in terms of orientation. Indeed, the (100)-oriented supercrystal had a λ_{100} = 505 nm (Figure 3b), whereas the (111)-oriented supercrystal exhibited a reflectance peak at λ_{111} = 578 nm (Figure 3d).

-Figure 3-

To account for the photonic properties observed, we calculated the photonic bands for a perfect fcc supercrystal comprising TRD particles joined by their hexagonal facets (Figure S11, Supporting Information).[27] In this calculation, we varied the refractive index to match the X-gap frequency (λ_{100} = 505 nm; Figure 3c), since the former is the only unknown parameter, because it depends on the amount of water absorbed during synthesis. For the ZIF-8, this calculation yielded a refractive index value of 1.535, which is consistent with previously reported values (inset in Figure 3c).[18]

As we mentioned earlier, the (111)-oriented supercrystal is singular, in that it is plastic and the orientation of its polyhedra is less regular than in the other two cases (*i.e.* only the <111> crystallites axes are preferentially oriented along the (111) supercrystal axis; Figure 1a). Consequently, such a structure presents photonic properties that do not respond to the photonic bands calculated for the aforementioned, perfect, close-packed fcc supercrystal. Thus, for the plastic fcc supercrystal, we had to model the TRDs as effective spheres with a diameter to be determined and a refractive index known from (001) reflection. We analyzed candidate sizes (ϕ_i) in the TRD that could be defined by joining diametrically opposing singular points on the surface (*e.g.* facet centers and corners) and that depend on the truncation of the particle (Figures S12,13, Supporting Information). Spheres of these diameters arranged in a close-packed fcc define lattice parameters $a_i = \phi_i\sqrt{2}$ and corresponding filling fractions. We examined the photonic bands of such lattices to determine the effective diameter at which the photonic gap at

the L-point in reciprocal space would match the experimentally measured value (λ_{111} = 578 nm). We concluded that the best fit is ϕ_5, which is the distance between the corner of opposing square facets (Inset to Figure 3e). The corresponding photonic band structure is shown in Figure 3e, and the spectrum of reflectance, in Figure 3d, where the accordance can be observed.

In conclusion, we have reported the self-assembly of TRD ZIF-8 crystals into well-ordered fcc supercrystals. These monolithic structures comprise monodisperse crystalline particles and, when no additional CTAB is added to the colloidal solution, the <111> ZIF-8 particle direction orients as the (111) supercrystal direction. We demonstrated that the entropically-favored (111) orientation of these ZIF-8 supercrystals can be forced through the (100) orientation - and even the (110) orientation - by increasing the concentration of CTAB in the colloidal solution. To the best our knowledge, this is the first reported example of orientation control in self-assembled polyhedral particles. Moreover, it is one of only a few examples demonstrating orientation control in colloidal crystals. Given that the ability to manipulate supercrystal orientation is important not only for MOFs, but for all colloidal crystals, our method should provide a powerful tool for pore-alignment, property tuning and/or crystal-orientation engineering.

Experimental Section

Materials and characterization: All chemical reagents and solvents were purchased from Sigma Aldrich and used as received without further purification. De-ionized (DI) water was obtained from a Milli-Q water purification system. Field-emission scanning electron microscopy (FE-SEM) images were collected on a scanning electron microscope (FEI Magellan 400L XHR) at acceleration voltage of 1.0 kV, using PDMS-coated aluminum-tape as support. The size of crystals was calculated from FE-SEM images by averaging the diameter of 200 particles from images of different areas of the same samples. XRPD measurements were done on an X'Pert PRO MPDP analytical diffractometer, λ_{Cu} = 1.5406 Å (PANalytical). Volumetric N_2 sorption

isotherms were collected at 77 K using an ASAP 2020 HD (Micromeritics). The reflectance spectra were taken with a Hyperion 2000 FT-IR microscope coupled to a Vertex 80 Spectrometer (both from Bruker) with a 15× Schwarzschild standard objective, tungsten lamp (in the Vertex 80) and a Si-diode detector.

Synthesis of truncated rhombic dodecahedral (TRD) ZIF-8 crystals with t = 0.63: A solution of 0.3 g of $Zn(OAc)_2 \cdot 2H_2O$ in 5 mL of DI water was added into a solution of 1.56 g of 2-MiM and 0.40 mg cetyltrimethylammonium bromide (CTAB) in 5 mL of DI water, and the resulting mixture was homogenized by stirring it for 15 s. Then, the mixture was let at room temperature for 2 h to form TRD ZIF-8 crystals with t = 0.63. The resulting ZIF-8 particles were washed three times with DI water upon centrifugation at 9000 r.p.m. in 50 mL Falcon tubes. The collected wet pellets were finally re-dispersed at a concentration of 50 mg/mL in DI water or in aqueous CTAB solution with varying concentrations from 1 to 4 mg/mL. Note that to prevent aggregation, the particles were dispersed while they were still wet.

Formation of the ZIF-8 supercrystals: The desired substrates (glass microscope slides, SEM pins, and Powder X-ray diffraction (PXRD) substrate) were initially washed with water and ethanol, and dried with a pressurized N_2 gun. Then, polydimethylsiloxane (PDMS) was mixed with the curing agent with a mass ratio of 10:1, and the resulting mixture was applied to the corresponding substrate and cured for 15 min at 120 ^oC. Then, 40 μL of the ZIF-8 colloidal solution was dropped on the PDMS coated surface and let in the oven to dry at 120 ^oC.

Supporting Information

Supporting Information is available from the Wiley Online Library or from the author.

Acknowledgements

This work was supported by the Spanish MINECO (projects PN MAT2015-65354-C2-1-R, MAT2015-68075-R); the Catalan AGAUR (project 2014 SGR 80); the Comunidad de Madrid PHAMA_2.0 (S2013/MIT-2740); the ERC, under the EU-FP7 (ERC-Co 615954); and the CERCA Program/Generalitat de Catalunya. ICN2 is supported by the Severo Ochoa program

from Spanish MINECO (Grant No. SEV-2017-0706). JAP acknowledges an FPI grant. Y. L. acknowledges the China Scholarship Council (CSC) for scholarship support.

Received: ((will be filled in by the editorial staff))
Revised: ((will be filled in by the editorial staff))
Published online: ((will be filled in by the editorial staff))

References

[1] S. Haussühl, *Physical Properties of Crystals: An Introduction*, Willey-VCH Verlag GmbH & Co. KGaA, Weinheim, Germany, **2007**.

[2] N.T. Nesbitt, M.J. Naughton, *Ind. Eng. Chem. Res.* **2017**, *56*, 10949.

[3] M.H. Huang, S. Mao, H. Feick, H. Yan, Y. Wu, H. Kind, E. Weber, R. Russo, P. Yang, *Science*. **2001**, *292*, 1897.

[4] D.P. Norton, A. Goyal, J.D. Budai, D.K. Christen, D.M. Kroeger, E.D. Specht, Q. He, B. Saffian, M. Paranthaman, C.E. Klabunde, D.F. Lee, *Science* **1996**, *274*, 755.

[5] K. Nomura, H. Ohta, K. Ueda, T. Kamiya, M. Hirano, H. Hosono, *Science* **2003**, *300*, 1269.

[6] Z. Pan, H.L. Lai, F.C. Au, X. Duan, W. Zhou, W. Shi, N. Wang, C.S. Lee, N.B. Wong, S.T. Lee, S. Xie, *Adv. Mater.* **2000**, *12*, 1186.

[7] a) R.S. Wagner, W.C. Ellis, *Appl. Phys. Lett.* **1964**, *4*, 89; b) E.I. Givargizov, *J. Cryst. Growth.* **1975**, *31*, 20.

[8] R.Q. Zhang, Y. Lifshitz, S.T. Lee, *Adv. Mater.* **2003**, *15*, 635.

[9] G. Cao, D., Liu, *Adv. Colloid Interface Sci.* **2008**, *136*, 45.

[10] Z. Lai, G. Bonilla, I. Diaz, J.G. Nery, K. Sujaoti, M.A. Amat, E. Kokkoli, O. Terasaki, R.W. Thompson, M. Tsapatsis, D.G. Vlachos, *Science* **2003**, *300*, 456.

[11] M.Y. Jeon, D. Kim, P. Kumar, P.S. Lee, N. Rangnekar, P. Bai, M. Shete, B. Elyassi, H.S. Lee, K. Narasimharao, S.N. Basahel, *Nature* **2017**, *543*, 690.

[12] Special issue on metal-organic framework materials. *Chem. Soc. Rev.* **2014**, *43*, 5415.

[13] Special issue on metal-organic frameworks and porous polymers – current and future challenges. *Chem. Soc. Rev.* **2017**, *46*, 3104.

[14] E. Biemmi, C. Scherb, T. Bein, *J. Am. Chem. Soc.* **2007**, *129*, 8054.

[15] D. Zacher, A. Baunemann, S. Hermes, R.A. Fischer, *J. Mater. Chem.* **2007**, *17*, 2785.

[16] O. Shekhah, M. Eddaoudi, *Chem. Commun*. **2013**, *49*, 10079.

[17] P. Falcaro, K. Okada, T. Hara, K. Ikigaki, Y. Tokudome, A.W. Thornton, A.J. Hill, T. Williams, C. Doonan, M. Takahashi, *Nat. Mater.* **2017**, *16*, 342.

[18] C. Avci, I. Imaz, A. Carné-Sánchez, J.A. Pariente, N. Tasios, J. Pérez-Carvajal, M.I. Alonso, A. Blanco, M. Dijkstra, C. López, D. Maspoch, *Nat. Chem*. **2018**, *10*, 78.

[19] J. Henzie, M. Grünwald, A. Widmer-Cooper, P. L. Geissler, P. Yang, *Nature Mater.* **2012**, *11*, 131.

[20] P.F. Damasceno, M. Engel, S.C. Glotzer, *Science* **2012**, *337*, 453.

[21] C. Jin, M.A. McLachlan, D.W. McComb, R.M. De la Rue, N.P. Johnson, *Nano Lett*. **2005**, *5*, 2646.

[22] Y. Zhong, L. Wu, H. Su, K.S. Wong, H., Wang, *Opt. Express*. **2006**, *14*, 6837.

[23] Y., Yin, Z.Y. Li, Y. Xia, *Langmuir* **2003**, *19*, 622.

[24] S.H. Im, Y.T. Lim, D.J. Suh, O.O., Park, *Adv. Mater.* **2002**, *14***,** 1367.

[25] N.V. Dziomkina, G.J. Vancso, *Soft Matter*. **2005**, *1*, 265.

[26] P. D. García, J. F. Galisteo-López, C. López, *Appl. Phys. Lett.* **2005**, *87*, 201109.

[27] S.G. Johnson, J.D. Joannopoulos, *Opt. Express*. **2001**, *8*, 173.

Avci *et al.*, Figure 1

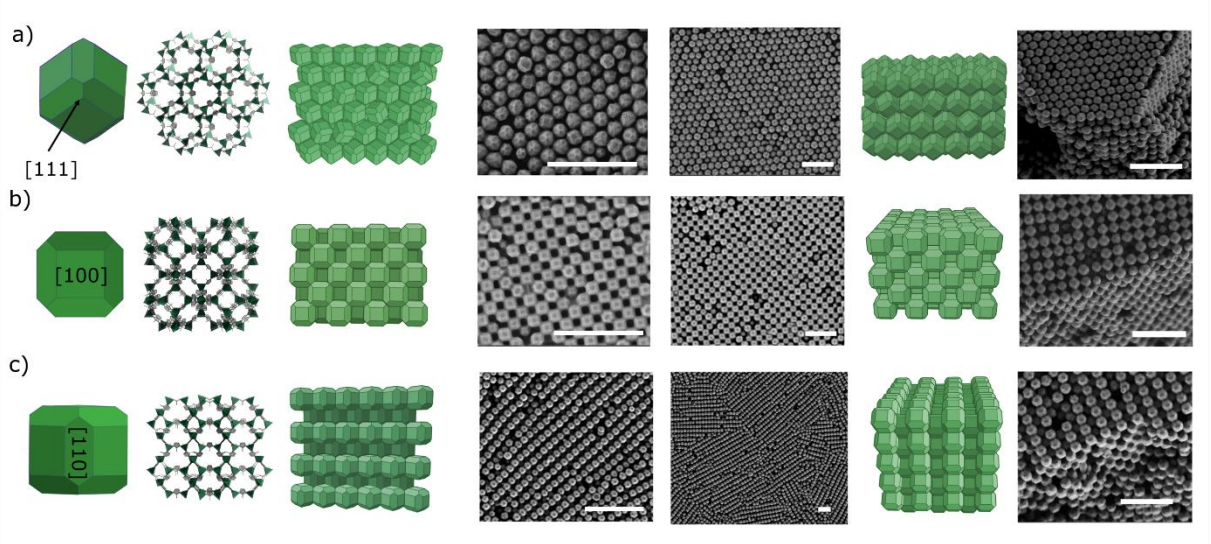

Figure 1. Formation of (a) (111)-, (b) (100)- and (c) (110)-oriented fcc supercrystals of TRD ZIF-8 particles. Each section contains (from left to right) a schematic view of a single TRD ZIF-8 particle oriented along the corresponding plane; a view of the oriented crystal structure of ZIF-8; a schematic view of the packing of the supercrystals, and corresponding FESEM images; and a schematic view of the 3D packing of the supercrystals, and corresponding FESEM image. Scale bars are 2 mm (4th column) and 1 mm (5th and 7th columns).

Avci *et al.*, Figure 2

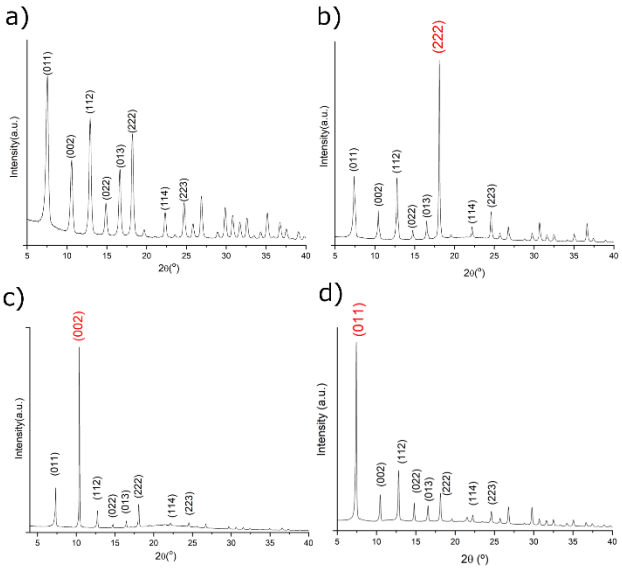

Figure 2. Powder X-ray diffraction (PXRD) for (a) the disordered ZIF-8 monolith and for the (b) (111)-, (c) (100)- and (d) (110)-oriented supercrystals.

Avci *et al.*, Figure 3

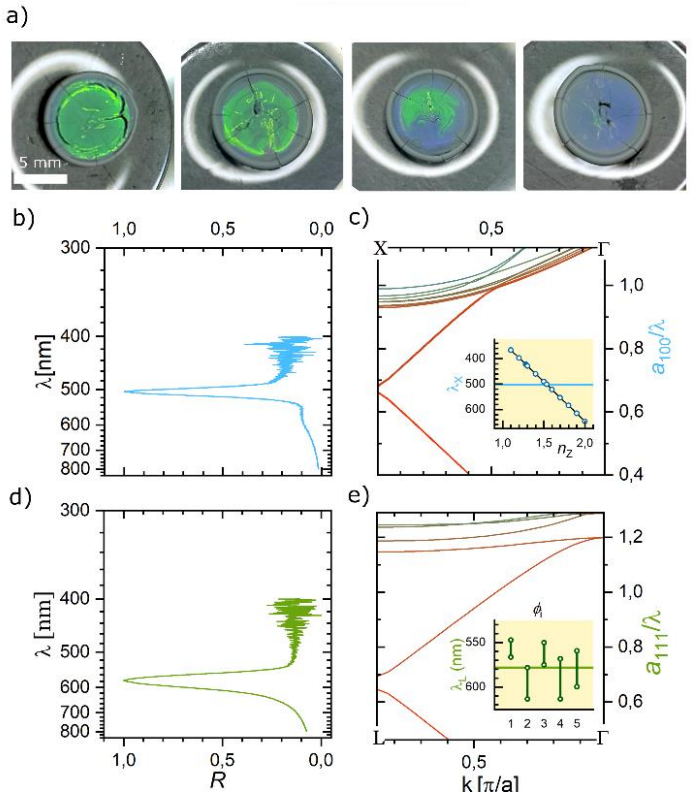

Figure 3. (a) Change in color of the supercrystals obtained upon increasing the CTAB concentration (left to right: 1 mg/mL, 2 mg/mL, 2.5 mg/mL and 3 mg/mL). Note that the photo on the far left corresponds to a (111)-oriented supercrystal, whereas the one on the right corresponds to a (100)-oriented supercrystal. The two intermediate photos correspond to mixtures of the two orientations, showing that the (100)-domains start at the perimeter, and then propagate to the center of the monolith, with increasing CTAB concentration. (b-e) Normalized specular optical reflectance-plots from (100) (b) and (111) (d) arrangements, and the corresponding photonic band-structures in the ΓX (c) and ΓL (e) directions. The insets in panels c) and e) show the photonic gap-positions λ_X and λ_L as functions of refractive index (c) and mean particle size $\boldsymbol{\phi_i}$, respectively.

Control on the mesoscale self-assembly of (111)-, (100)- and (110)-oriented face-centered cubic supercrystals of Metal-Organic Framework (MOF) particles by adjusting the amount of surfactant (CTAB) used is described. It is reported that, by controlling the orientation of supercrystals made of the colloidal polyhedral MOF ZIF-8, porous ZIF-8 crystals on surfaces are oriented. Further, these supercrystals behave as photonic crystals whose properties depend on their growth orientation.

Civan Avci, Yang Liu, Jose Angel Pariente, Alvaro Blanco, Cefe Lopez,* Inhar Imaz,* Daniel Maspoch*

Template-free, Surfactant-Mediated Orientation of Self-Assembled Supercrystals of Metal-Organic Framework Particles